Journal of Low Temperature Physics
https://doi.org/10.1007/s10909-020-02452-z

Low-Temperature Magnetic Properties and Magnetocaloric Effect of Fe–Zr–Cu Amorphous Alloys

Weiming Yang[1] · Wenyu Li[1] · Chao Wan[1,2] · Juntao Huo[2] · Jinyong Mo[1] · Haishun Liu[1] · Baolong Shen[3]

Received: 15 December 2019 / Accepted: 21 March 2020

Abstract

In this work, low-temperature magnetic properties and magnetocaloric properties of $Fe_{91-x}Zr_9Cu_x$ ($x=0.0$, 0.4 and 1.0) amorphous ribbons were investigated. It was found that the Curie temperature (T_C) of the ribbons increases with Cu content from 210 (for $x=0$) to 218 K (for $x=0.4$), and decreases to 214 K with the further of 1.0% Cu. The values of the maximum magnetic entropy change $(-\Delta S_M)_{max}$ were found to be 2.63, 2.75 and 2.88 J kg^{-1} K^{-1} for the $Fe_{91-x}Zr_9Cu_x$ ($x=0.0$, 0.4 and 1.0) amorphous ribbons, respectively, under the field of 50 kOe. The corresponding refrigeration capacity (RC) values of the $Fe_{91-x}Zr_9Cu_x$ ($x=0.0$, 0.4 and 1.0) amorphous ribbons are 114, 121 and 120 J kg^{-1}, respectively. These values are comparable to those obtained for the previously studied ternary Fe-based amorphous alloys. These results demonstrate that an appropriate amount of Cu substitution can enhance the $(-\Delta S_M)_{max}$ and RC of Fe-based amorphous alloys. These Fe-based amorphous alloys are promising for application as low-temperature magnetic refrigerants and multi-functional materials.

Keywords Magnetocaloric effect · Fe-based amorphous alloys · Magnetic entropy change · Refrigeration capacity

✉ Juntao Huo
huojuntao@nimte.ac.cn

✉ Haishun Liu
liuhaishun@126.com

[1] School of Mechanics and Civil Engineering, State Key Laboratory for Geomechanics and Deep Underground Engineering, China University of Mining and Technology, Xuzhou 221116, People's Republic of China

[2] Key Laboratory of Magnetic Materials and Devices, Ningbo Institute of Materials Technology and Engineering, Chinese Academy of Sciences, Ningbo 315201, People's Republic of China

[3] School of Materials Science and Engineering, Southeast University, Nanjing 211189, People's Republic of China

Published online: 19 May 2020

1 Introduction

Due to its great merits such as environmental friendliness and relatively high efficiency, magnetic refrigeration technology based on the magnetocaloric effect (MCE) has attracted intense research interest [1–3]. To date, several intermetallic compounds such as Gd–Si–Ge [4], La–Ca–Mn–O [5], Ni–Mn–Ga [6], La–Fe–Si [7], Mn–Fe–P–As [8], Ni–Mn–Sn [9] have been found to display a giant MCE due to their first-order magneto-structural phase transitions. Unfortunately, these phase transitions are accompanied by large thermal and magnetic hysteresis that reduces the operational frequency of the refrigeration applications based on these materials [10]. By contrast, soft magnetic materials are well known to show low hysteresis because irreversible entropy can be avoided during their magnetization and/or demagnetization. Therefore, the development of magnetic refrigerants based on soft magnetic materials can also allow the replacement of superconducting magnets with permanent magnets for the generation of external magnetic fields [11]. Fe-based amorphous alloys are some of the most well-known soft magnetic systems. Unlike crystalline materials in which the constituent atoms are at thermodynamic equilibrium, Fe-based amorphous alloys are metastable materials in far-from-equilibrium states [12] and show many properties that are desirable for magnetic refrigerants such as low cost, high electrical resistivity [13, 14], high corrosion resistance [15], tunability of the transition temperature by alloying [16], good mechanical properties [17] and negligible magnetic hysteresis.

Among the Fe-based amorphous alloys, Fe–Zr alloy ribbons have recently attracted much interest [18] because their ferromagnetic to paramagnetic (FM-PM) transition temperature (T_C, Curie temperature) can be easily tuned to the desired temperature range through the doping of other elements while not affecting many of the favorable MCE properties of the Fe–Zr parent compound. Even though many studies have been performed on the Fe–Zr alloy ribbons doped with Ti, Cr, Mn, Sn, Co, Ni, Y and/or B [10, 19–25], no investigations of Cu-doped Fe–Zr materials have been reported. Since the magnetic and structural properties are strongly linked by the *c/a* lattice parameter ratio [26–28] and the density of the 3*d* electrons at the Fermi level [29], replacement of Fe by Cu should give rise to site- and element-specific changes in the electronic and magnetic properties of the Fe–Zr alloy.

In this work, we have fabricated Fe–Zr–Cu amorphous ribbon samples and investigated their magnetic and MCE properties at temperatures in the vicinity of the T_C. The use of ternary magnetocaloric Fe-based amorphous alloys simplifies the study of the physics underlying the MCE in these materials. This work will also provide guidance for further research on MCE of amorphous alloys that are promising magnetic refrigerants.

2 Experimental

Ingots with the nominal compositions of $Fe_{91-x}Zr_9Cu_x$ ($x = 0.0$, 0.4 and 1.0) were prepared by arc melting pure elements (99.99 wt%) in an argon atmosphere. To ensure homogeneity, every ingot was remelted five times. Amorphous ribbons with

width of approximately 1 mm and thickness of 30 μm were prepared by the single-roller melt-spinning method with a surface speed of 40 m/s under argon atmosphere. The amorphous nature of the melt-spun ribbons was verified by X-ray diffraction (XRD, D8-Discover, Bruker) with Cu Kα radiation, and thermal analysis was performed using a differential scanning calorimeter (DSC, 404 F3, Netsch) at a heating rate of 40 K/min. The temperature and field dependences of the DC magnetization were measured using the magnetic measurement component of a physical property measurement system (MPMS). The temperature dependence of the magnetization (*M–T*) was measured under a field of 0.02 T during the heating process from 10 to 300 K. The isothermal magnetization (*M–H*) curves were measured at various temperatures under a field of 5 T.

3 Results and Discussion

The XRD patterns of $Fe_{91-x}Zr_9Cu_x$ ($x=0.0$, 0.4 and 1.0) alloys are shown in Fig. 1a. Typical halo peaks characteristic of amorphous materials are observed for each of the samples with no obvious diffraction peaks of crystalline phases, indicating the amorphous nature of the fabricated $Fe_{91-x}Zr_9Cu_x$ ($x=0.0$, 0.4 and 1.0) alloys. The DSC curves of these alloys are presented in Fig. 1b, and the observed exothermic peaks correspond to crystallization by heating. The onset temperatures of the crystallization event (T_x) of the $Fe_{91-x}Zr_9Cu_x$ ($x=0.0$, 0.4 and 1.0) alloys are 842, 830 and 805 K, respectively, showing that T_x decreases with increasing Cu content. The T_x of $Fe_{91-x}Zr_9Cu_x$ ($x=0.0$, 0.4 and 1.0) are much higher than the corresponding T_C values (see below), indicating that these alloys are stable in the range of practical application temperatures. The DSC thermograms presented in Fig. 1b show two exothermic maxima at approximately 850 K and 900 K. The first peak is attributed to the crystallization of α-Fe, and the second peak is related to the formation of Fe_3Zr [30].

Figure 2a shows the magnetic hysteresis loops of the $Fe_{91-x}Zr_9Cu_x$ ($x=0.0$, 0.4 and 1.0) amorphous alloys at 10 K. It is observed that M_s increases with increasing Cu substitution, reaches the maximum value at $x=0.4$, and then decreases with further Cu substitution. Among the investigated Fe-based amorphous alloys, the $Fe_{90.6}Zr_9Cu_{0.4}$ alloy exhibits the highest M_s of 125 emu/g, in agreement with the previous report [25]. It is known that M_s is determined by the *c*/*a* lattice parameter ratio and the density of the 3*d* electrons at the Fermi level [29]. Since Cu has a positive heat of mixing with Fe atoms [31, 32], the Cu and Fe atoms would repel each other in the Cu-doped alloys, and so that an appropriate addition of Cu will promote the bonding of Fe–Fe pairs [33], and will lead to the increase in the number of the nearest-neighbor Fe atoms. According to Heisenberg theory [34], the atomic magnetic moment is assumed to depend on the number of the nearest-neighbor Fe atoms. Therefore, an appropriate Cu substitution ($x=0.4$) for Fe can also increase the saturation magnetization [35]. With excessive additions of 1.0% Cu, the effect of the reduction in the Fe concentration may become more dominant, resulting in the decrease in M_s. The results for the temperature dependence of the magnetization (*M–T*) of the $Fe_{91-x}Zr_9Cu_x$ ($x=0.0$, 0.4

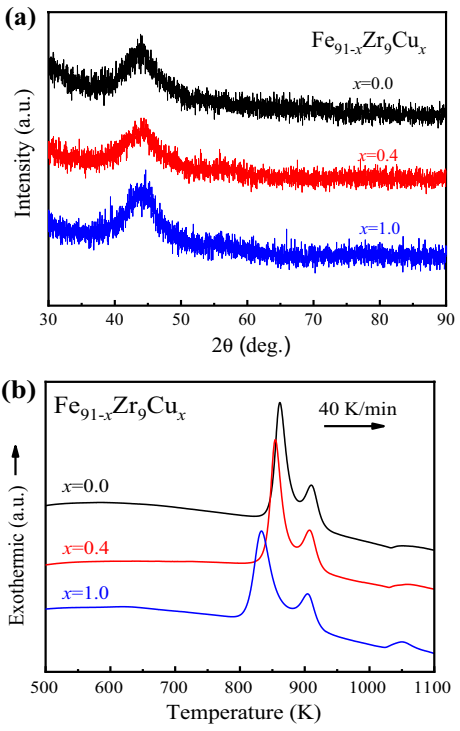

Fig. 1 **a** XRD patterns of $Fe_{91-x}Zr_9Cu_x$ ($x=0.0$, 0.4 and 1.0) ribbons; **b** DSC heating curves of $Fe_{91-x}Zr_9Cu_x$ ($x=0.0$, 0.4 and 1.0) ribbons (Color figure online)

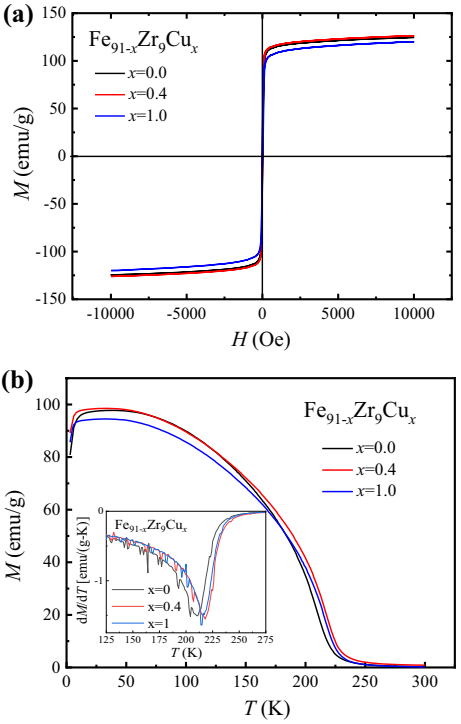

Fig. 2 **a** Hysteresis loops of $Fe_{91-x}Zr_9Cu_x$ ($x=0.0$, 0.4 and 1.0) amorphous alloys at 10 K; **b** Temperature dependence of magnetization under a magnetic field of 200 Oe and at zero field. The inset displays the thermal derivative of the magnetization data as a function of temperature (Color figure online)

and 1.0) amorphous alloys measured at an applied field of 200 Oe in the temperature range of 10–300 K are also presented in Fig. 2b. The T_c can be determined from the temperature at the minimum of the curve of dM/dT plotted versus T, and the obtained T_c values for $Fe_{91-x}Zr_9Cu_x$ were approximately 210, 218 and 214 K for $x = 0.0$, 0.4 and 1.0, respectively. This is mainly due to the sensitivity of the Fe–Fe exchange interaction to the interatomic distance that gives rise to fluctuations in the magnitude and can also reverse the sign of the magnetic exchange integral [17]. An appropriate addition of Cu can promote the bonding of the Fe–Fe pairs and leads to the increase in the number of the nearest-neighbor Fe atoms. Thus, a substitution of a small amount of Fe with Cu ($x = 0.4$) leads to an increase in T_c. This result is similar to those obtained for other Fe-rich amorphous alloys with minor Cu additions [36]. It should be noted that as shown in Fig. 2b, the magnetization (M) decreases with temperatures decreasing below 10 K. This is attributed to the fact that the higher Zr content in the present set of alloys enhances the ferromagnetic interaction [21] and spin-glass behavior [37].

Together with careful investigations of $M(T)$, we also measured the $M(H)$ curves at the temperatures in the vicinity of T_C, as shown in Fig. 3a–c for the $Fe_{91-x}Zr_9Cu_x$ samples with $x = 0.0$, 0.4 and 1.0, respectively. Similar to the $M(T)$ data, it was found that increasing temperature reduces M. At a given temperature, M increases gradually with increasing magnetic field H, with a rapid rise in M observed at $H < 15$ kOe. Notably, the M in the FM region does not reach saturation even at magnetic fields as high as 50 kOe. Similar results were also observed in many other amorphous alloys [21, 38, 39]. Due to the competition between the thermal disorder and the exchange interactions favoring magnetic order, the FM nonlinear $M(H)$ curves become linear when the sample enters the PM region. This magnetic phase separation is observed more clearly when M^2 is plotted versus H/M in Arrott plots [40]. The nonlinear parts in the low-field region at the temperatures below and above T_C are driven towards two opposite directions, as shown in Fig. 3d–f, revealing the FM-PM separation. According to the mean-field theory for long-range FM order [25], the M^2 versus H/M isotherms for a system with long-range FM order give a set of straight lines passing through the origin in the vicinity of T_C. Thus, the absence of the linearity suggests the existence of a short-range FM order in the alloy ribbons. Additionally, it is observed that the plots of H/M versus M^2 (not shown) exhibit positive curvatures in the vicinity of T_C, revealing that the samples undergo a second-order magnetic phase transition [41, 42].

Based on the results derived from M-T curves, the isothermal magnetization curves (M–H) were measured near the T_c. The magnetic entropy change (ΔS_M) as a function of temperature is used to characterize the MCE of a magnetic material and can be calculated from the M–H curves using the Maxwell relation given by [43]:

$$\Delta S_M = \mu_0 \int_0^{H_{max}} \left(\frac{\partial M}{\partial T}\right)_H dH \tag{1}$$

where μ_0 is the permeability of vacuum and H_{max} is the maximum applied field. The magnetic field with maximal value of 5 T was used in our experiments. To derive

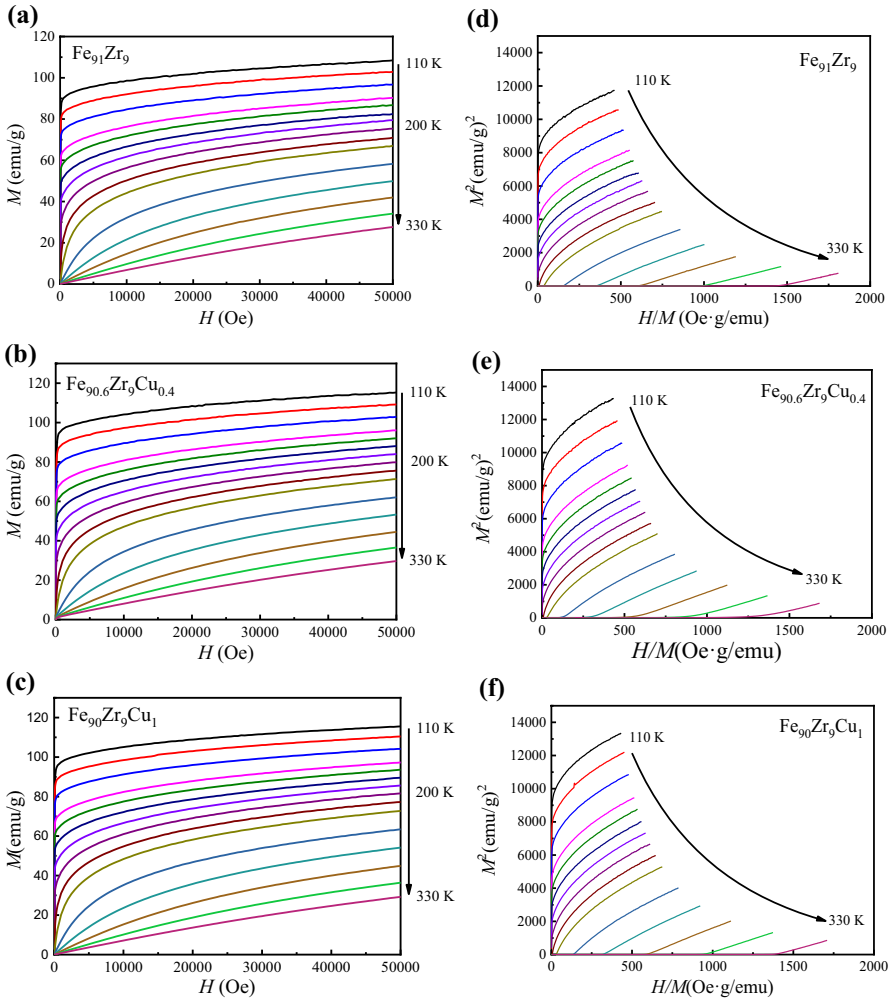

Fig. 3 **a–c** $M(H)$ and **d–f** M^2 versus H/M curves for $Fe_{91-x}Zr_9Cu_x$ ($x=0.0$, 0.4 and 1.0) at a temperature close to T_c (Color figure online)

the temperature dependence of ΔS_M, the integral was evaluated numerically according to

$$\Delta S_M(T_i, H) = \frac{\int_0^H M(T_i, H)\mathrm{d}H - \int_0^H M(T_{i+1}, H)\mathrm{d}H}{T_i - T_{i+1}} \tag{2}$$

Using the isothermal M–H curves obtained at various temperatures, we evaluated the ΔS_M associated with H variations according to Eq. (2). Figure 4a–c shows the temperature dependence of the $-\Delta S_M(T)$ for the H fields of up to 50 kOe. It is observed that each $-\Delta S_M(T)$ curve has a maximum value $-\Delta S_{max}$ in

the vicinity of the FM–PM transition temperature T_c and that an increase in H enhances $-\Delta S_M$ and $-\Delta S_{max.}$ For $H=10$ kOe, the $-\Delta S_{max.}$ values were approximately 0.74, 0.75, and 0.80 J kg^{-1} K^{-1} for the $Fe_{91-x}Zr_9Cu_x$ alloys with $x=0.0$, 0.4 and 1.0, respectively. For $H=50$ kOe, these values increased up to 2.63, 2.75, and 2.88 J kg^{-1} K^{-1}, respectively. The temperatures (T^{pk}) at which the peak entropy change values ($-\Delta S_M{}^{pk}$) are obtained are close to the T_c because of the nature of second-order phase transition.

Refrigerant capacity (*RC*) is another important parameter that characterizes the refrigerant efficiency of the material. Here, we estimated the *RC* value as the product of the peak entropy change and the full width at half maximum of the peak [44]:

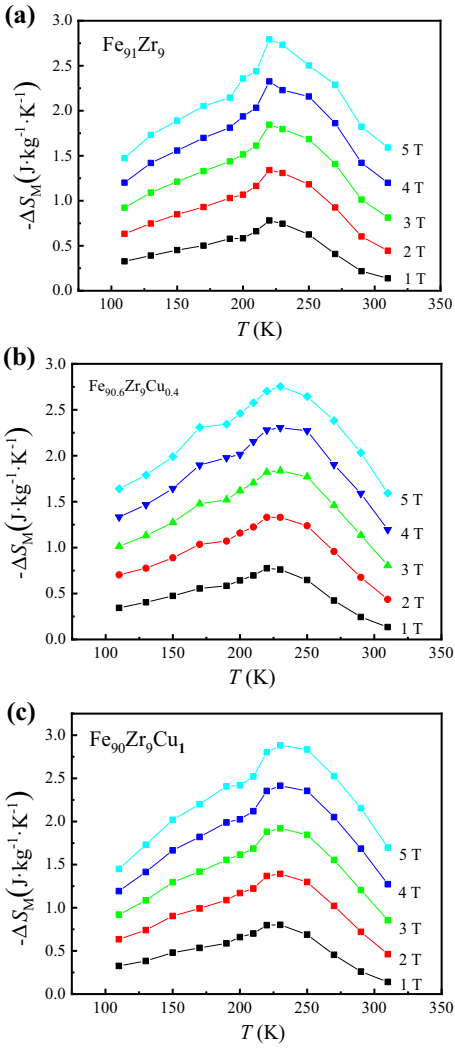

Fig. 4 $-\Delta S_M(T)$ curves for the $Fe_{91-x}Zr_9Cu_x$ amorphous alloy samples (**a** $x=0.0$, **b** $x=0.4$, and **c** $x=1.0$) at H field ranging from 10 to 50 kOe (Color figure online)

$$\mathrm{RC}_{\mathrm{FWHM}} = -\Delta S_{\mathrm{M}}^{\mathrm{pk}} \times \delta T_{\mathrm{FWHM}} \tag{3}$$

where δT_{FWHM} is defined as the temperature interval of the full width at half maximum of $-\Delta S_{\mathrm{M}}$. Figure 5 shows the results of the examination of the *RC* dependence on *H* for the alloy ribbons. It is observed that the *RC* values of the $Fe_{91-x}Zr_9Cu_x$ amorphous alloys with $x = 0.0$, 0.4 and 1.0 were approximately 114, 121, and 120 J kg^{-1} under *H* of 20 kOe, and were 250, 264, and 261 J kg^{-1} under *H* of 50 kOe, respectively. Thus, *RC* increases with increasing *H*, while at a given field, the *RC* values first increase with increasing Cu substitution, and then decrease with further Cu substitution. It is clear that the values of T_c, *RC*, and ΔS_{M} can be tuned by the change in the Cu content of the Fe–Zr alloy ribbons. Table 1 presents the comparison of the T_c, *RC*, and $(-\Delta S_{\mathrm{M}})_{\mathrm{max}}$ values of the samples produced in this work with the results obtained for the Fe-based alloys in previous studies reported in the literature.

For a better evaluation and comparison of the obtained experimental results to the literature, theoretical analysis is necessary to understand the dependence of the maximum magnetic entropy change on the magnetic field strength. It has been shown that the relationship between the magnetic field and the magnetic entropy change is described by a power law in the magnetic field strength [51]:

$$\left|\Delta S_{\mathrm{M}}^{\mathrm{pk}}\right| \propto AH^n \tag{4}$$

The values of the "*n*" parameter and the correlation coefficients for the data obtained for the samples studied in this work were calculated by comparing the experimentally obtained data to the fitted data. The $\left|\Delta S_{\mathrm{M}}^{\mathrm{pk}}\right|$ values of the $Fe_{91-x}Zr_9Cu_x$ ($x = 0.0$, 0.4 and 1.0) ribbons were fitted in the magnetic field strength range of 0–50 kOe using Eq. (4), and as shown in Fig. 6, the experimental data were found to be in a good agreement with fitted data. The "*n*" value predicted by mean-field theory is approximately 2/3 [52], while it is observed from Fig. 6 that the values of the "*n*" exponent for the $Fe_{91-x}Zr_9Cu_x$ ($x = 0.0$, 0.4 and 1.0) ribbons were 0.77, 0.80, and 0.79, respectively. The deviation of these values from the expected mean-field

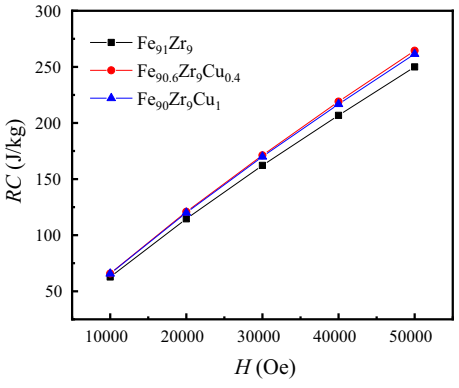

Fig. 5 Field dependence of the *RC* for $Fe_{91-x}Zr_9Cu_x$ ($x = 0.0$, 0.4 and 1.0) amorphous alloys (Color figure online)

Table 1 Curie temperature, and magnetic entropy changes under applied fields of 1.5 T and 5 T, and the refrigerant capacity under applied fields of 2 T and 5 T for the present and typical reported ternary Fe-based amorphous alloys

Compositions (at.%)	T_C (K)	$-\Delta S_M$ (J kg^{-1} K)		RC_{FWHM} (J kg^{-1})		References
		1.5 T	5 T	2 T	5 T	
$Fe_{91}Zr_9$	210	–	2.63	114	250	This work
$Fe_{90.6}Zr_9Cu_{0.4}$	218	–	2.75	121	264	
$Fe_{90}Zr_9Cu_1$	214	–	2.88	120	261	
$Fe_{88}Zr_8B_4$	285	–	3.30	159	435	[45]
$Fe_{91}Zr_7B_2$	230	–	2.80	148	435	
$Fe_{80}Cr_8B_{12}$	328	1.00	2.59	–	–	[46]
$Fe_{77}Cr_8B_{15}$	375	1.18	2.98	–	–	
$Fe_{84}Nb_7B_9$	299	1.44	–	–	–	[47]
$Fe_{79}Nb_7B_{14}$	372	1.07	–	–	–	
$Fe_{73}Nb_7B_{20}$	419	0.97	–	–	–	
$Fe_{86}Y_5Zr_9$	284	0.89	–	–	–	[48]
$Fe_{81}Y_{10}Zr_9$	470	1.12	–	–	–	
$Fe_{70}Mn_{10}B_{20}$	438	1.00	–	117 (1.5 T)	–	[49]
$Fe_{65}Mn_{15}B_{20}$	340	0.87	–	98 (1.5 T)	–	
$Fe_{60}Mn_{20}B_{20}$	210	0.60	–	83 (1.5 T)	–	
$Fe_{56}Mn_{24}B_{20}$	162	0.50	–	68 (1.5 T)	–	
$Fe_{85}Zr_{10}B_5$	300	1.39	–	–	–	[10]
$Fe_{82}Mn_8Zr_{10}$	210	–	2.78	–	–	[50]
$Fe_{84}Mn_6Zr_{10}$	218	–	2.29	–	–	
$Fe_{86}Mn_4Zr_{10}$	228	–	2.51	–	–	
$Fe_{80}Mn_{10}Zr_{10}$	195	–	2.33	–	–	

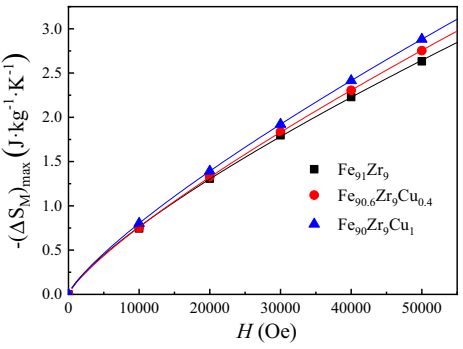

Fig. 6 Magnetic field dependence of the maximum magnetic entropy changes for $Fe_{91-x}Zr_9Cu_x$ ($x=0.0$, 0.4 and 1.0) amorphous ribbons. The solid lines show the results of fitting to $\left|\Delta S_M^{pk}\right| \propto AH^n$ (Color figure online)

theory value may be due to the local inhomogeneities or nanocrystallization present in the $Fe_{91-x}Zr_9Cu_x$ ($x=0.0$, 0.4 and 1.0) ribbons.

4 Conclusion

In this work, the low-temperature magnetic properties and magnetocaloric effect of $Fe_{91-x}Zr_9Cu_x$ ($x = 0$, 0.4 and 1) ribbons have been investigated. The amorphous structure and stability of these alloys have been verified by XRD and DSC measurements. With the addition of 0.4% Cu, the Curie temperature of the ribbons increased from 210 to 218 K and then decreased to 214 K with a further increase in Cu content to 1.0%. The maximum magnetic entropy change $(-\Delta SM)max$ values were found to be 2.63, 2.75 and 2.88 J kg^{-1} K^{-1} for the $Fe_{91-x}Zr_9Cu_x$ ($x = 0.0$, 0.4 and 1.0) amorphous ribbons, respectively, under a maximum field of 50 kOe. The corresponding refrigeration capacity values of the $Fe_{91-x}Zr_9Cu_x$ ($x = 0.0$, 0.4 and 1.0) amorphous ribbons are 114, 121 and 120 J kg^{-1}, respectively, and both T_c and $-\Delta S_M^{pk}$ can be improved by the addition of Cu. Thus, these alloys are promising materials for the development of high-performance amorphous solid-state refrigerants.

Acknowledgments This work was supported by the National Natural Science Foundation of China (Nos. 51631003, 51871237 and 51771217) and Xuzhou Key Research and Development Program (KC17015).

References

1. V. Franco, J. Blázquez, B. Ingale, A. Conde, Mater. Res. **42**, 305 (2012)
2. O. Gutfleisch, M.A. Willard, E. Brück, C.H. Chen, S. Sankar, J.P. Liu, Adv. Mater. **23**, 821 (2011)
3. Q. Luo, B. Schwarz, N. Mattern, J. Shen, J. Eckert, AIP Adv. **3**, 032134 (2013)
4. V.K. Pecharsky, J.K.A. Gschneidner, Phys. Rev. Lett. **78**, 4494 (1997)
5. Z.B. Guo, Y.W. Du, J.S. Zhu, H. Huang, W.P. Ding, D. Feng, Phys. Rev. Lett. **78**, 1142 (1997)
6. F.-X. Hu, B.-G. Shen, J.-R. Sun, Appl. Phys. Lett. **76**, 3460 (2000)
7. F.-X. Hu, B.-G. Shen, J.-R. Sun, Z.H. Cheng, G.H. Rao, X.-X. Zhang, Appl. Phys. Lett. **78**, 3675 (2001)
8. O. Tegus, E. Brück, K. Buschow, F. De Boer, Nature **415**, 150 (2002)
9. Y. Zhang, Q. Zheng, W. Xia, J. Zhang, J. Du, A. Yan, Scr. Mater. **104**, 41 (2015)
10. Y. Wang, X. Bi, Appl. Phys. Lett. **95**, 262501 (2009)
11. V. Pecharsky, K. Gschneidner Jr., J. Appl. Phys. **86**, 565 (1999)
12. J.Q. Wang, Y.H. Liu, M.W. Chen, G.Q. Xie, D.V. Louzguine-Luzgin, A. Inoue, J.H. Perepezko, Adv. Funct. Mater. **22**, 2567 (2012)
13. R. Caballero-Flores, V. Franco, A. Conde, K. Knipling, M. Willard, Appl. Phys. Lett. **96**, 182506 (2010)
14. S. Meng, H. Ling, Q. Li, J. Zhang, Scr. Mater. **81**, 24 (2014)
15. S.J. Pang, T. Zhang, K. Asami, A. Inoue, Acta Mater. **50**, 489 (2002)
16. W.M. Yang, H.S. Liu, L. Xue, J.W. Li, C.C. Dun, J.H. Zhang, Y.C. Zhao, B.L. Shen, J. Magn. Magn. Mater. **335**, 172 (2013)
17. W. Yang, H. Liu, Y. Zhao, A. Inoue, K. Jiang, J. Huo, H. Ling, Q. Li, B. Shen, Sci. Rep. **4**, 6233 (2014)
18. X.D. Liu, X.B. Liu, Z. Altounian, J. Non-Cryst, Solids **351**, 604 (2005)
19. P. Álvarez, J.S. Marcos, P. Gorria, L.F. Barquín, J.A. Blanco, J. Alloys Compd. **504**, S150 (2010)
20. Y. Fang, C. Yeh, C. Hsieh, C. Chang, H. Chang, W. Chang, X. Li, W. Li, J. Appl. Phys. **105**, 07A910 (2009)

21. D. Mishra, M. Gurram, A. Reddy, A. Perumal, P. Saravanan, A. Srinivasan, Mater. Sci. Eng. B **175**, 253 (2010)
22. T. Phan, N. Dan, T. Thanh, N. Mai, T. Ho, S. Yu, A.-T. Le, M. Phan, J. Korean. Phys. Soc. **66**, 1247 (2015)
23. Y. Moon, S. Min, K. Kim, S. Yu, Y. Kim, K. Kim, J. Magn. **10**, 142 (2005)
24. K. Kim, S. Min, J. Zidanic, S. Yu, J. Magn. **12**, 133 (2007)
25. T. Dang, Y. Yu, P. Thanh, N. Yen, N. Dan, T.-L. Phan, A. Grishin, S. Yu, J. Appl. Phys. **113**, 213908 (2013)
26. P. Bhobe, K. Priolkar, P. Sarode, Phys. Rev. B **74**, 224425 (2006)
27. A. Ayuela, J. Enkovaara, R. Nieminen, J. Phys. Condens. Matter. **14**, 5325 (2002)
28. A. Zayak, W. Adeagbo, P. Entel, K. Rabe, Appl. Phys. Lett. **88**, 111903 (2006)
29. A. Zayak, P. Entel, K. Rabe, W. Adeagbo, M. Acet, Phys. Rev. B **72**, 054113 (2005)
30. N.M.N. Zfirubovfi, H. Kronmiiller, Mater. Sci. Eng. A **151**, 205 (1992)
31. W. Yang, H. Liu, X. Fan, L. Xue, C. Dun, B. Shen, J. Non-Cryst. Solids **419**, 65 (2015)
32. A. Takeuchi, A. Inoue, Mater. Trans. **46**, 2817 (2005)
33. L. Dou, H. Liu, L. Hou, L. Xue, W. Yang, Y. Zhao, C. Chang, B. Shen, J. Magn. Magn. Mater. **358**, 23 (2014)
34. W. Heisenberg, Z. Phys. **49**, 619 (1928)
35. J.E. Gao, H.X. Li, Z.B. Jiao, Y. Wu, Y.H. Chen, T. Yu, Z.P. Lu, Appl. Phys. Lett. **99**, 052504 (2011)
36. K. Sarlar, E. Civan, I. Kucuk, J. Non-Cryst. Solids **471**, 169 (2017)
37. J. Li, L. Xue, W. Yang, C. Yuan, J. Huo, B. Shen, Intermetallics **96**, 90 (2018)
38. W. Sheng, J.-Q. Wang, G. Wang, J. Huo, X. Wang, R.-W. Li, Intermetallics **96**, 79 (2018)
39. K.S. Kim, Y.S. Kim, J. Zidanic, S.G. Min, S.C. Yu, Phys. Status Solidi (a) **204**, 4096 (2007)
40. V. Provenzano, A.J. Shapiro, R.D. Shull, Nature **429**, 853 (2004)
41. B. Banerjee, Phys. Lett. **12**, 16 (1964)
42. T.L. Phan, N.H. Dan, T.D. Thanh, N.T. Mai, T.A. Ho, S.C. Yu, A.-T. Le, M.H. Phan, J. Korean Phys. Soc. **66**, 1247 (2015)
43. T. Hashimoto, T. Numasawa, M. Shino, T. Okada, Cryogenics **21**, 647 (1981)
44. K. Gschneidner Jr., V. Pecharsky, Annu. Rev. Mater. Sci. **30**, 387 (2000)
45. P. Álvarez, P. Gorria, J.S. Marcos, L.F. Barquín, J.A. Blanco, Intermetallics **18**, 2464 (2010)
46. V. Franco, A. Conde, L.F. Kiss, J. Appl. Phys. **104**, 033903 (2008)
47. S.-G. Min, K.-S. Kim, S.-C. Yu, K.-W. Lee, Mater. Sci. Eng. A **449**, 423 (2007)
48. K. Kim, S. Min, S. Yu, S. Oh, Y. Kim, K. Kim, J. Magn. Magn. Mater. **304**, e642 (2006)
49. R. Caballero-Flores, V. Franco, A. Conde, L.F. Kiss, J. Appl. Phys. **108**, 073921 (2010)
50. S. Min, K. Kim, S. Yu, H. Suh, S. Lee, J. Appl. Phys. **97**, 10M310 (2005)
51. V. Franco, A. Conde, Int. J. Refrig **33**, 465 (2010)
52. H. Oesterreicher, F. Parker, J. Appl. Phys. **55**, 4334 (1984)